Response to the submission (#1741) of KDD 2024

Table A: The existing representative Riemannian batch normalization methods, where M, V, CM, and CV represent the Mean, Variance, Controllable Mean, and Controllable Variance, respectively.

Methods	**Statistics**	**CM**	**CV**	**Scenarios**
SPDNetBN [7]	M	√	N/A	SPD Manifolds-AIM
ManifoldNorm [8]	M + V	×	×	Riemannian homogeneous space
SPDBN [R1]	M + V	√	√	SPD Manifolds-AIM
SPDMBN [R2]	M + V	√	√	SPD Manifolds-AIM
Ours（SPDNetCBN)	M + V	√	√	SPD manifolds-LCM

Table B: Accuracy comparison (%) of different RBN methods on the HDM05 and large scale NTU-60 [R3] datasets.

Methods	**HDM05**	**NTU-60 [R3]**
SPDNetBN [7]	64.89 ± 1.40	52.89 ± 1.22
ManifoldNorm [8]	57.26 ± 0.89	50.60 ± 0.52
SPDBN [R1]	65.60 ± 0.80	54.07 ± 0.41
SPDMBN [R2]	66.58 ± 0.58	54.59 ± 1.01
Ours (SPDNetCBN)	**69.85 ± 0.52**	**55.93 ± 0.41**

The results given in Table B further verify the efficacy of our CBN over other RBN methods on the HDM05 and large-scale NTU-60 datasets.

Table C: Summary of Riemannian operators related to AIM and LCM.

Manifold	**AIM on the SPD manifold**	**Metric on the Cholesky manifold**
Metric	AIM: $\mathcal{T}_X\mathcal{M} \times \mathcal{T}_X\mathcal{M}$	LCM: $\sum_{i>j} \mathbf{A}_{ij}\mathbf{B}_{ij} + \sum_{j=1}^{d} \mathbf{A}_{jj}\mathbf{B}_{jj}\mathbf{L}_{jj}^{-2}$
Distance	$\frac{1}{2}\|\log(X_1^{-\frac{1}{2}} X_2 X_1^{-\frac{1}{2}})\|_{\mathrm{F}}$	$\{\| \lfloor \mathbf{L} \rfloor - \lfloor \mathbf{A} \rfloor \|_{\mathrm{F}}^2 + \| \log\mathbb{D}(\mathbf{L}) - \log\mathbb{D}(\mathbf{A}) \|_{\mathrm{F}}^2\}^{\frac{1}{2}}$
Logarithmic Map (LM)	$Q^{\frac{1}{2}}\log(Q^{\frac{1}{2}} X Q^{-\frac{1}{2}})Q^{\frac{1}{2}}$	$\lfloor \mathbf{A} \rfloor - \lfloor \mathbf{L} \rfloor + \mathbb{D}(\mathbf{L})\log\{\mathbb{D}(\mathbf{L})^{-1}\mathbb{D}(\mathbf{A})\}$
Exponential Map (EM)	$X^{\frac{1}{2}}\exp(X^{\frac{1}{2}} Q X^{-\frac{1}{2}})X^{\frac{1}{2}}$	$\lfloor \mathbf{A} \rfloor + \lfloor \mathbf{L} \rfloor + \mathbb{D}(\mathbf{A})\exp\{\mathbb{D}(\mathbf{L})\mathbb{D}(\mathbf{A})^{-1}\}$
Parallel Transport (PT)	$(X_2 X_1^{-1})^{\frac{1}{2}} Q (X_2 X_1^{-1})^{\frac{1}{2}}$	$\lfloor \mathbf{A} \rfloor + \mathbb{D}(\mathbf{L}_2)\mathbb{D}(\mathbf{L}_1)^{-1}\mathbb{D}(\mathbf{A})$
Riemannian Mean (RM)	No closed form	Closed form

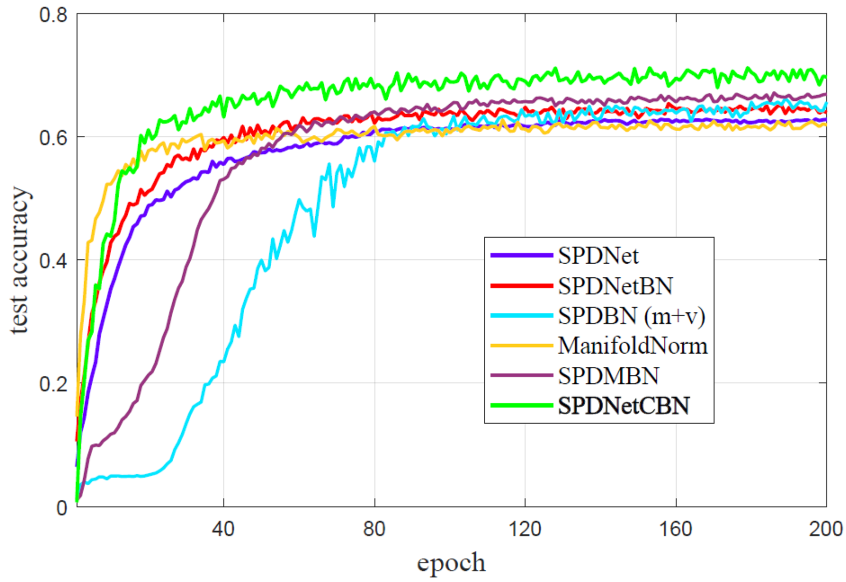

Figure A: Convergence performance of different RBN methods on the HDM05 dataset.

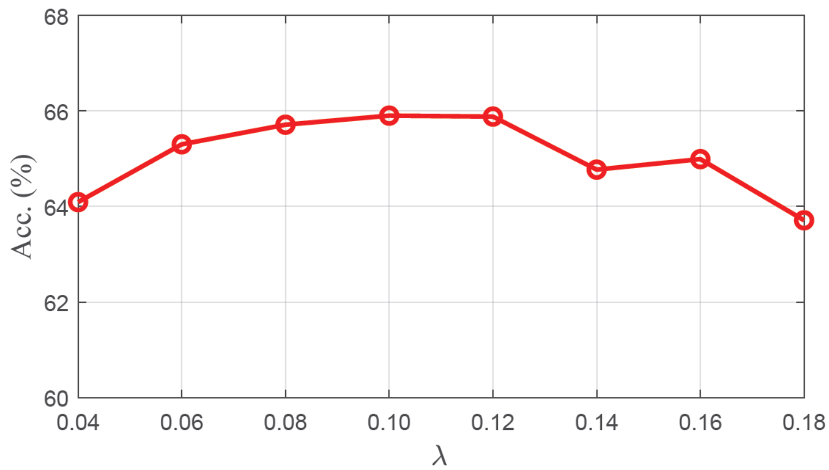

Figure B: The accuracy of our method versus the value of λ on the MAMEM dataset.

In the proposed CBN module, the weight λ (Alg.1 in the main paper) is the only hyperparameter. From Fig. B, we can see that our method seems to be insensitive to this parameter, and the suggested proper value range is 0.08~0.12.

Table D: The accuracy of our method versus different Gaussian noise on the MAMEN dataset.

Gaussian Noise	None	$\mathcal{N}(0, 0.1)$	$\mathcal{N}(0, 0.2)$	$\mathcal{N}(0, 0.3)$	$\mathcal{N}(0, 0.5)$	$\mathcal{N}(0, 1.0)$	$\mathcal{N}(0, 2.0)$
Acc. (%)	**64.95**	64.38	64.09	63.25	61.67	59.84	56.67

From Table D, it can be found that within a reasonable range, our method has certain robustness to the added Gaussian noise. Note that the Gaussian noise is added to the original signals.

References:

[R1] Kobler, R. J., Hirayama, J. I., & Kawanabe, M. Controlling the fréchet variance improves batch normalization on the symmetric positive definite manifold. In *ICASSP*, 2022, pp. 3863-3867.

[R2] Kobler, R., Hirayama, J. I., Zhao, Q., & Kawanabe, M. SPD domain-specific batch normalization to crack interpretable unsupervised domain adaptation in EEG. In *NeurIPS*, 2022, pp. 6219-6235.

[R3] Shahroudy, A., Liu, J., Ng, T. T., & Wang, G. Ntu rgb+d: A large scale dataset for 3d human activity analysis. In *CVPR*, 2016, pp. 1010-1019.